Journal of Vacuum Science and Technology A

RESEARCH ARTICLE | FEBRUARY 07 2024

# Reliable electrical performance of $\beta$-$Ga_2O_3$ Schottky barrier diode at cryogenic temperatures

**Special Collection:** Gallium Oxide Materials and Devices

Haolan Qu ; Wei Huang ; Yu Zhang ; Jin Sui ; Jiaxiang Chen ; Baile Chen ; David Wei Zhang; Yuangang Wang; Yuanjie Lv ; Zhihong Feng; Xinbo Zou



*J. Vac. Sci. Technol. A* 42, 023418 (2024)
https://doi.org/10.1116/6.0003298

JVST A
Journal of Vacuum Science & Technology A
ARTICLE
pubs.aip.org/avs/jva

# Reliable electrical performance of $\beta$-$Ga_2O_3$ Schottky barrier diode at cryogenic temperatures

Cite as: J. Vac. Sci. Technol. A **42**, 023418 (2024); doi: 10.1116/6.0003298
Submitted: 11 November 2023 · Accepted: 11 January 2024 ·
Published Online: 7 February 2024

View Online Export Citation CrossMark

Haolan Qu,[1,2,3] Wei Huang,[4] Yu Zhang,[1,2,3] Jin Sui,[1,2,3] Jiaxiang Chen,[1,2,3] Baile Chen,[1] David Wei Zhang,[4] Yuangang Wang,[5] Yuanjie Lv,[5] Zhihong Feng,[5] and Xinbo Zou[1,6,a)]

## AFFILIATIONS

[1]School of Information Science and Technology, ShanghaiTech University, Shanghai 201210, People's Republic of China
[2]Shanghai Institute of Microsystem and Information Technology, Chinese Academy of Sciences, Shanghai 200050, People's Republic of China
[3]School of Microelectronics, University of Chinese Academy of Sciences, Beijing 100049, People's Republic of China
[4]School of Microelectronics, Fudan University, Shanghai 200433, People's Republic of China
[5]The National Key Laboratory of Application Specific Integrated Circuit (ASIC), Hebei Semiconductor Research Institute, Shijiazhuang, Hebei 050051, People's Republic of China
[6]Shanghai Engineering Research Center of Energy Efficient and Custom AI IC, Shanghai 200031, People's Republic of China

**Note:** This paper is part of the Special Topic Collection on Gallium Oxide Materials and Devices.
[a)]**Author to whom correspondence should be addressed:** zouxb@shanghaitech.edu.cn



## ABSTRACT

Electrical and trap characteristics of a large-size ($2 \times 2$ mm$^2$) $\beta$-$Ga_2O_3$ Schottky barrier diode (SBD) from 50 to 350 K have been reported. The ideality factor ($n$) decreases from 1.34 to nearly unity as temperature rises from 50 to 350 K, demonstrating near-ideal Schottky characteristics. The leakage current at cryogenic temperature (100 K) was significantly suppressed, indicating excellent off-state blocking performance at low temperatures. The weak temperature dependence of the carrier concentration ($N_S$) and Schottky barrier height ($\Phi_B$) infers stable electrical characteristics of the $\beta$-$Ga_2O_3$ SBD. The stressed current density-voltage ($J$-$V$) and on-the-fly measurements reveal reliable dynamic performance under harsh low temperature conditions. Via deep-level transient spectroscopy, an electron trap, which is related to the dynamic performance instability and Lorentzian hump in low frequency noise spectra, is revealed for a $\beta$-$Ga_2O_3$ epilayer. The study reveals enormous potential of the utilization of a large-size $\beta$-$Ga_2O_3$ SBD for extreme temperature environments.



## I. INTRODUCTION

$\beta$-$Ga_2O_3$ is attracting increasing attention for power conversion applications due to its ultrawide bandgap (4.9 eV), large critical electric field (8 MV/cm), and high electron mobility (250 cm$^2$/V s).[1–3] A $\beta$-$Ga_2O_3$ Schottky barrier diode (SBD) incorporating a novel junction termination extension has reportedly exhibited a high breakdown voltage of over 2.5 kV, a specific on-resistance of 5.9 m$\Omega$ cm$^2$, and a high Baliga's power figure of merit surpassing 1 GW/cm$^2$.[4]

Several studies have reported the characteristics of the $\beta$-$Ga_2O_3$ SBD in extreme environments such as high reverse voltage stress,[5] high temperature,[6,7] neutron irradiation,[8–10] proton irradiation,[11] and electron irradiation.[12] Temperature-dependent on-resistance was derived from the forward current characteristics of a $\beta$-$Ga_2O_3$ SBD from 25 to 175 °C.[13] Decreased carrier lifetime and diffusion length with increasing fluences were also observed and documented for a $\beta$-$Ga_2O_3$ SBD after 1.5 MeV electron irradiation.[12]

Nevertheless, the characteristics of $\beta$-$Ga_2O_3$ SBDs at cryogenic temperatures have not been thoroughly investigated. Several issues still need to be solved before the implementation of the $\beta$-$Ga_2O_3$ SBD for cryogenic temperature applications, such as satellite electronics.[14]

(a) Compared with $\beta$-$Ga_2O_3$ SBD directly on a bulk material,[15,16] the $\beta$-$Ga_2O_3$ SBD fabricated on a high-quality epilayer has been regarded as a viable path to improve the electrical performance of devices. However, the static and dynamic performance of the $Ga_2O_3$ SBD with a homogeneous epilayer at cryogenic temperature is still unknown. The lack of such results would mask the potential of the $\beta$-$Ga_2O_3$ SBD for low temperature applications.

(b) There have been some studies reporting the dynamic performance of the $\beta$-$Ga_2O_3$ SBD by applying various forward and reverse stresses.[5,17,18] Forward stress up to 14 V has been applied to investigate the instability of turn-on voltage ($V_{th}$), on-resistance ($R_{on}$), and $n$.[17] However, the relationship among dynamic performance, low frequency noise, and specific deep-level trap in the $\beta$-$Ga_2O_3$ SBD at both cryogenic temperature and room temperature is still unavailable.

In this paper, the electrical and trap characteristics were investigated for a large-size ($2 \times 2\ mm^2$) $\beta$-$Ga_2O_3$ SBD at both room temperature and cryogenic temperature. Static electrical characteristics were studied by temperature-dependent capacitance-voltage ($C$-$V$) and current density-voltage ($J$-$V$) characteristics from 50 to 350 K. Dynamic performance and low frequency noise were applied to elucidate the impact of bulk traps at both room temperature and cryogenic temperature. Via deep-level transient spectroscopy (DLTS), an electron trap was discovered in the $\beta$-$Ga_2O_3$ epilayer. The comprehensive study paves a solid path toward practical applications of the large-size $\beta$-$Ga_2O_3$ SBD in extreme environments.

## II. RESULTS AND DISCUSSION

### A. Device and static characteristics

Figure 1(a) illustrates the schematic cross section of the $\beta$-$Ga_2O_3$ SBD. The device structure contains a 7 $\mu$m-thick $\beta$-$Ga_2O_3$ epilayer grown on a $\beta$-$Ga_2O_3$ substrate. Ti/Au and Ni/Au were deposited as the backside ohmic contact and the square Schottky contact ($2 \times 2\ mm^2$), respectively.

Figure 1(b) depicts the linear fitting of forward $J$-$V$ characteristics. $V_{th}$, defined at a current density of 1 A/cm$^2$, is 0.78 V at 300 K, and it increases to 1.06 V at 100 K due to the increasing barrier at cryogenic temperature. Meanwhile, $R_{on}$ at 95 mA decreases from 0.14 $\Omega\,cm^2$ at 300 K to 0.12 $\Omega\,cm^2$ at 100 K. The forward current density of the $\beta$-$Ga_2O_3$ SBD satisfies the thermionic emission model,[19]

$$J = J_S\left(e^{\frac{qV}{nkT}} - 1\right), \tag{1}$$

$$J_S = A^* T^2 e^{\frac{-q\Phi_{B0}}{kT}}, \tag{2}$$

where $q$ represents the elementary charge, $k$ is the Boltzmann constant, and $A^*$ represents the Richardson coefficient. Meanwhile, $n$ and $J_S$ can be extracted from the slope and intercept of the linear region of $ln(J)$-$V$ :[20]

$$n = \frac{q}{kT}\left(\frac{dV}{dln(J)}\right). \tag{3}$$

Figure 1(c) plots the $ln(J_S/T^2) - 1/kT$, which exhibits high linearity. $\Phi_{B0}$ can be determined from the slope of linear fitting, and $q\Phi_{B0}$ is extracted to be 0.75 eV. Temperature-dependent $n$ is plotted

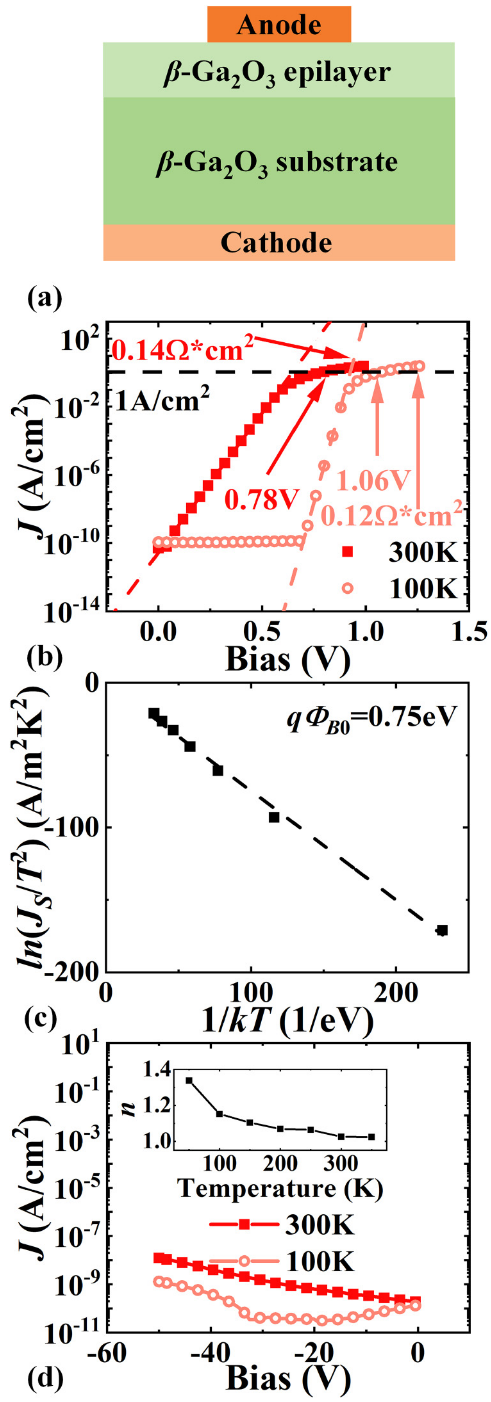


**FIG. 1.** (a) Schematic cross section of the $\beta$-$Ga_2O_3$ SBD. (b) Temperature-dependent forward $J$-$V$ characteristics in the logarithmic scale and linear fitting of the thermionic emission model. (c) Arrhenius plot to obtain the effective Schottky barrier height at 0 K ($\Phi_{B0}$). (d) Temperature-dependent reverse $J$-$V$ characteristics in the logarithmic scale. Inset: temperature-dependent $n$.

in the inset in Fig. 1(d). The decrease in $n$ from 1.34 to 1.02 with rising temperature from 50 to 350 K is attributed to the temperature-enhanced current transport process occurring at the interface of the metal and semiconductor.[20] Meanwhile, $n$ is also an indicator of Schottky barrier inhomogeneity. The high value of $n$ is attributed to the inhomogeneity caused by interface defects/states, dislocations, and thin interfacial layers between the metal and semiconductor.[15] The extracted $n$ is close to 1 at both cryogenic temperature and room temperature, indicating that the device exhibits insignificant Schottky barrier inhomogeneity and reliable near-ideal Schottky characteristics.[21] Figure 1(d) depicts the reverse $J$-$V$ characteristics. The leakage current density of the $\beta$-$Ga_2O_3$ SBD is $1.22 \times 10^{-8}$ A/cm$^2$ at a reverse bias of $-50$ V at 300 K, and it decreases to $1.28 \times 10^{-9}$ A/cm$^2$ at 100 K, confirming outstanding off-state blocking performance at cryogenic temperatures.

Figure 2(a) shows the temperature-dependent $C$-$V$ characteristics with a frequency ($f$) of 1 MHz. The capacitance decreases from 42.64 nF/cm$^2$ at 300 K to 36.82 nF/cm$^2$ at 100 K with zero bias. As shown in Fig. 2(b), $V_{bi}$ and $\Phi_B$ can be derived from the linear fitting of $1/C^2$-$V$ characteristics by the following equations:[22]

$$\frac{1}{C^2} = \frac{2}{\varepsilon_r \varepsilon_0 q A^2 (N_d - N_a)} \left( V + V_{bi} - \frac{kT}{q} \right), \tag{4}$$

$$q\Phi_B = qV_{bi} + E_C - E_F = qV_{bi} - kTln\left(\frac{N_d - N_a}{N_C}\right), \tag{5}$$

where $\varepsilon_r$ and $\varepsilon_0$ are the relative and vacuum permittivity, respectively, $A$ is the anode area, $E_C$ is the conduction band minimum, $E_F$ is the Femi level, and $N_C$ is the effective density of states in the conduction band. As shown in Fig. 2(c), when the temperature rises from 50 to 350 K, $qV_{bi}$ moderately decreases from 0.69 to 0.47 eV, while $q\Phi_B$ slightly reduces from 0.70 to 0.65 eV, matching well with the decreasing $V_{th}$ and increasing $R_{on}$ at high temperature. Compared to $qV_{bi}$, $q\Phi_B$ has weak dependence on temperature, which is caused by the compensation of $E_C$–$E_F$.[22] $N_C$ exhibits a monotonically increasing trend with temperature, leading to a rising $E_C$–$E_F$, which restrains the influence of $qV_{bi}$ on $q\Phi_B$. As the temperature rises, the slight decrease in $q\Phi_B$ is associated with the reduction in the semiconductor bandgap.[23] Meanwhile, the value of $q\Phi_B$ extracted from $C$-$V$ characteristics is different from $q\Phi_{B0}$ extracted from $J$-$V$ characteristics due to the different definitions. It should be noted that $q\Phi_B$ extracted from $C$-$V$ represents the average Schottky barrier height and is temperature-dependent, while $q\Phi_{B0}$ extracted from $J$-$V$ refers to the effective Schottky barrier height at 0 K and is a temperature-independent specific value.[24] From the $n$, a small barrier inhomogeneity exists, leading to a less difference between the average Schottky barrier height and effective Schottky barrier height. As exhibited in the inset in Fig. 2(a), $N_d - N_a$ can be extracted to be $1.39 \times 10^{16}$ cm$^{-3}$ at 300 K from $C$-$V$ characteristics. Meanwhile, $N_d - N_a$ is measured to be $1.36 \times 10^{16}$ cm$^{-3}$ at 100 and 50 K, demonstrating the negligible carrier freezing-out issue.[25]

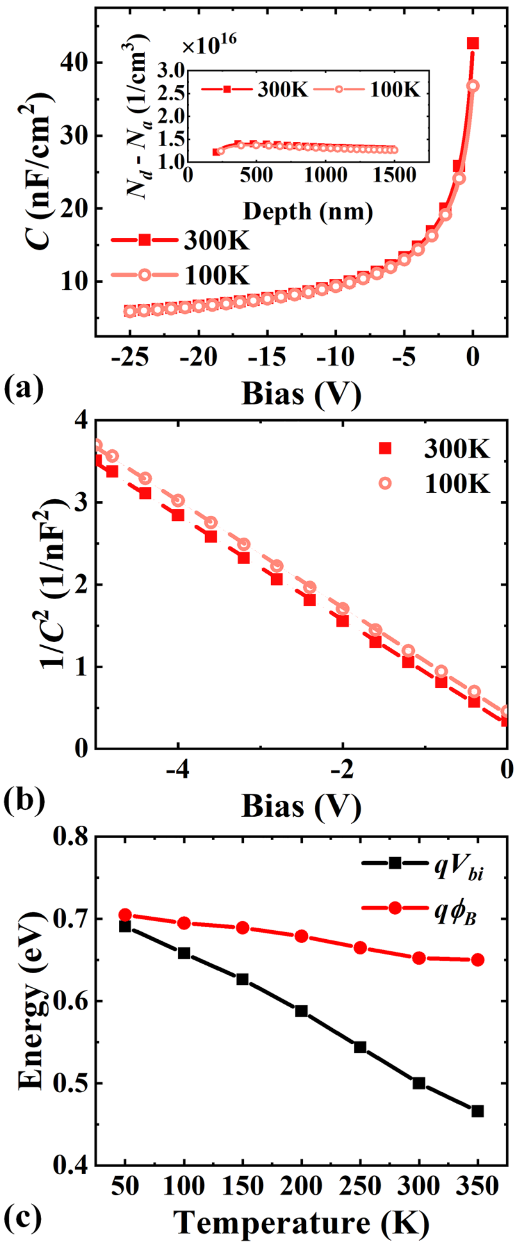


FIG. 2. (a) Temperature-dependent $C$-$V$ characteristics. Inset: carrier concentration ($N_d - N_a$). (b) Temperature-dependent $1/C^2 - V$ characteristics. (c) $\Phi_B$ and built-in voltage ($V_{bi}$).

## B. Dynamic characteristics

Stressed $J$-$V$ measurement is applied to study the dynamic performance of the $\beta$-$Ga_2O_3$ SBD at 300 and 100 K, as shown in Figs. 3(a) and 3(b). The inset in Fig. 3(a) shows the minor variation in $J$ when the device is exposed to an $U_s$ of $-100$ V, for various stressing durations. $J$-$V$ curves were positively shifted during the

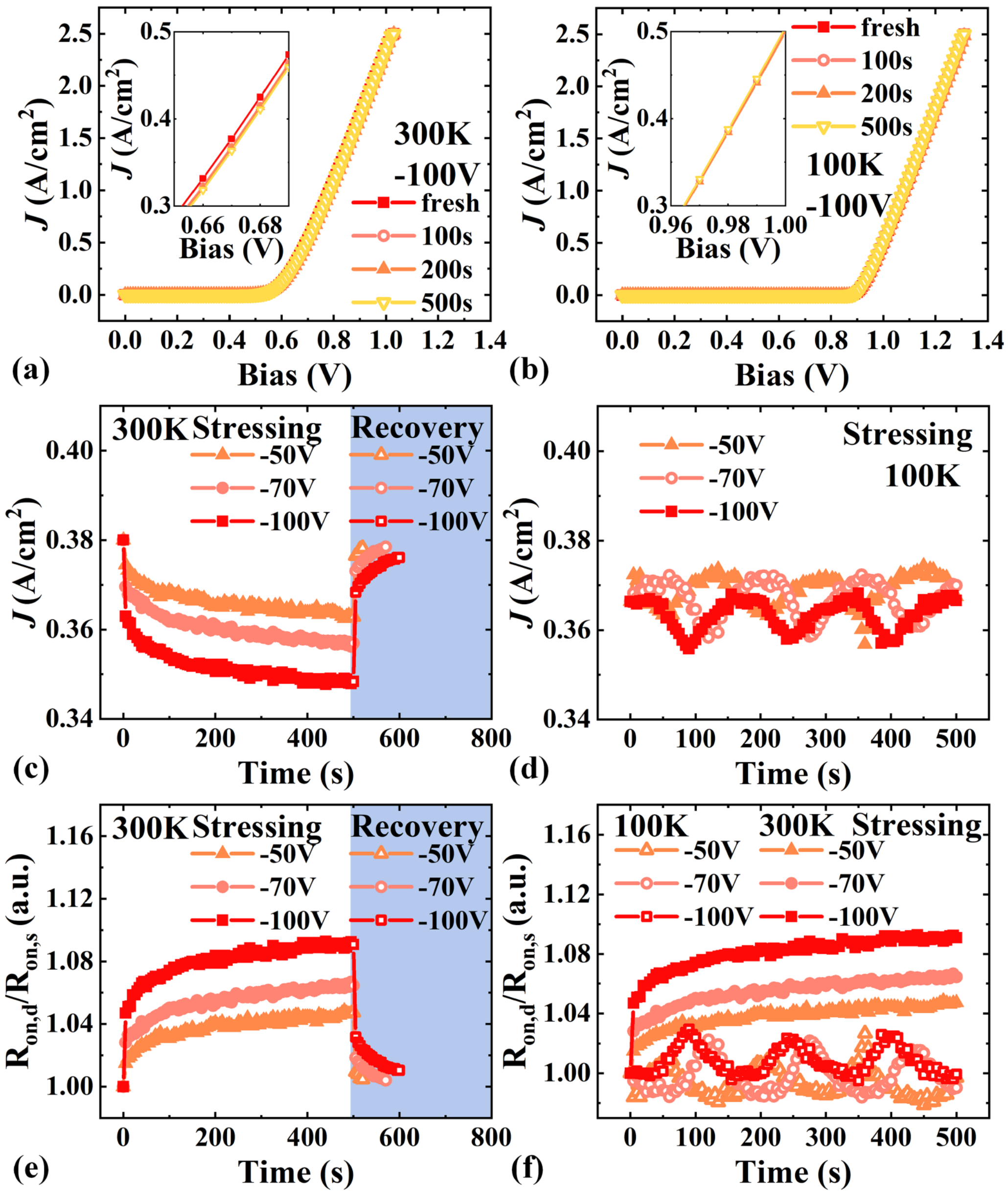


**FIG. 3.** Stressed *J-V* measurement with reverse stressing voltage ($U_s$) of −100 V (a) at 300 K and (b) at 100 K. Inset: partial amplification of stressed *J-V* characteristics. (c) *J* at measurement voltage ($U_m$) of 0.67 V at 300 K during the stressing process and recovery process. (d) *J* at an $U_m$ of 0.98 V at 100 K during the stressing process. (e) Dynamic on-resistance ratio at an $U_m$ of 0.67 V at 300 K during the stressing process and recovery process. (f) Dynamic on-resistance ratio at an $U_m$ of 0.67 V at 300 K and an $U_m$ of 0.98 V at 100 K during the stressing process.

stressing process, indicating an emission process of bulk trap at 300 K. However, as exhibited in the inset in Fig. 3(b), *J-V* curves remain stable during the same stressing process, inferring a reliable electrical performance at 100 K.

On-the-fly measurement is also performed to further investigate the dynamic performance of the $\beta$-$Ga_2O_3$ SBD at 300 and 100 K. Figure 3(c) shows the variation in *J* at 0.67 V when the device is exposed to various $U_s$, for a stressing time of 500 s. With increasing stressing time, *J* declines from 0.38 to 0.36 A/cm$^2$ for a reverse stressing voltage of −50 V. When $U_s$ is enhanced to −100 V, *J* decreases to 0.35 A/cm$^2$. For the recovery process (the shadow region), within 20 s, *J* gradually recovers from 0.36 to 0.38 A/cm$^2$ after the device is biased to the $U_s$ of −50 V for 500 s. When $U_s$ is enhanced to −100 V, *J* only recovers to 0.37 A/cm$^2$ within 20 s.

Compared to the monotonical reduction in $J$ at 300 K, $J$ fluctuates within a limited range around the original current density at 100 K, as shown in Fig. 3(d). At 300 K, the variation in $J$ is associated with the occupied state of bulk traps in the depletion region. With longer stressing time, the number of empty bulk traps rises, leading to increased $J$.[26] The variation in $J$ is also related to the change in $U_s$, for the depletion region is widened with enhanced $U_s$, which increases the number of empty bulk traps. At 100 K, the inertness of bulk traps leads to slight fluctuation of $J$.

Figures 3(e) and 3(f) show the dynamic on-resistance ratio as a function of stressing time at 300 and 100 K. The dynamic on-resistance ratio is defined as $R_{on,d}/R_{on,s}$, where $R_{on,d}$ and $R_{on,s}$ are the on-resistance measured in on-the-fly measurement and fresh state, respectively. When the device is exposed to $U_s$ of −50, −70, and −100 V for a stressing time of 500 s, the ratio is measured to be 1.05, 1.06, and 1.09 at 300 K, respectively, as exhibited in Fig. 3(e). Meanwhile, the ratio dramatically increases from 0 to 5 s, indicating that most of the bulk traps are emptied during the first 5 s. During the recovery process, as depicted in the shadow region of Fig. 3(e), the ratio can recover to a fresh state after recovery times of 20 and 70 s when $U_s$ is −50 V and −70 V at 300 K, respectively. However, after a recovery time of 100 s, the ratio only decreases to 1.01 when $U_s$ is −100 V, indicating that 100 s is not enough for $R_{on,d}$ to completely recover. Figure 3(f) depicts the ratio of 300 and 100 K during the stressing process. Compared to the results at 300 K, the ratio is limited to $1 \pm 0.03$ with all $U_s$ at 100 K. The small variation in the ratio demonstrates good dynamic switching performance of the $\beta$-$Ga_2O_3$ SBD at cryogenic temperature.

### C. Low frequency noise analysis

Figure 4 displays the low frequency noise characteristics of the $\beta$-$Ga_2O_3$ SBD at 300 and 100 K. Figures 4(a) and 4(b) depict the noise current density spectra at 300 and 100 K from 1 Hz to 10 kHz. The low frequency noise consists of flicker noise and Lorentzian noise, and $S_I$ spectra have a $1/f$ component caused by flicker noise and a $1/f^2$ component caused by Lorentzian noise.[27] As shown in Fig. 4(a), $S_I$ at 0.8 V is five or six orders of magnitude larger than $S_I$ at 0.5 V due to the high forward current density with high forward bias. A Lorentzian hump, which is associated with a generation-recombination center in the bulk of the $\beta$-$Ga_2O_3$ SBD, can be observed at 300 K. $S_I$ at 1.1 V is twelve or thirteen orders of magnitude larger than $S_I$ at 0.8 V, as exhibited in Fig. 4(b). At the fixed bias of 0.8 V, $S_I$ at 300 K is twelve or thirteen orders of magnitude larger than $S_I$ at 100 K. The large low frequency noise level is considered to be related to the large forward current density at high temperature.[28] Meanwhile, the Lorentzian hump disappears at 100 K. Figures 4(c) and 4(d) show $S_I f$ as a function of $f$ to eliminate the influence of the $1/f$ component. The Lorentzian hump in Fig. 4(c) could be acutely observed, indicating that bulk trap plays an important role in the electrical performance at room temperature. Nevertheless, as shown in Fig. 4(d), no Lorentzian hump could be found, inferring low activity of bulk trap at cryogenic temperature.

### D. DLTS measurement

Trap characteristics of the $\beta$-$Ga_2O_3$ SBD are investigated by DLTS measurement. Figure 5(a) exhibits a temperature-scanning

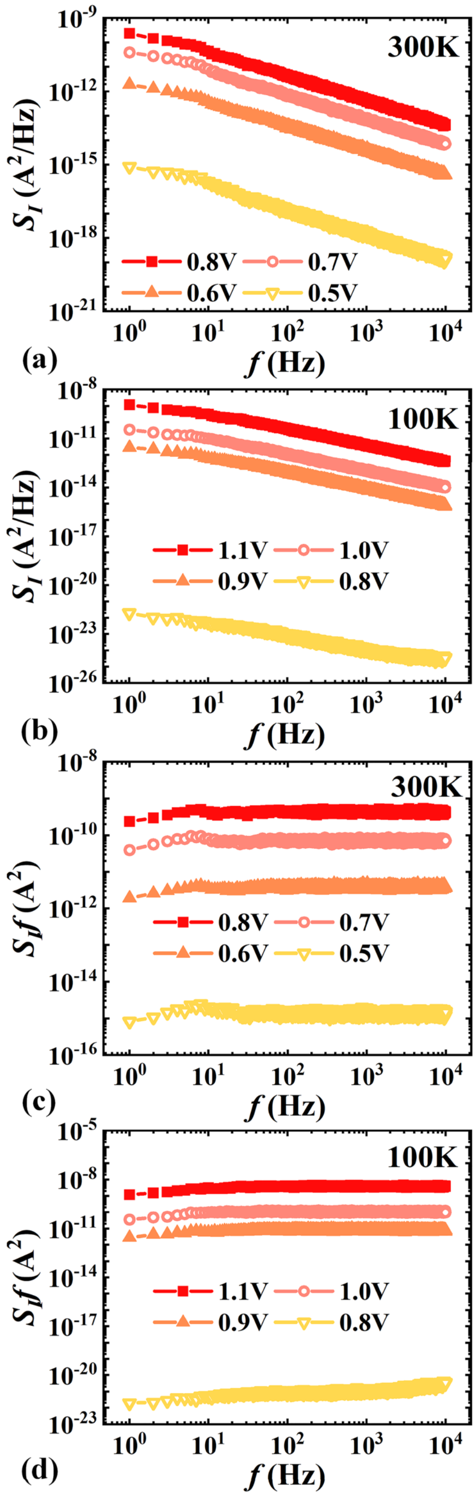


**FIG. 4.** Noise current density ($S_I$) spectra at (a) 300 and (b) 100 K. $S_I f$ as a function of $f$ at (c) 300 and (d) 100 K.

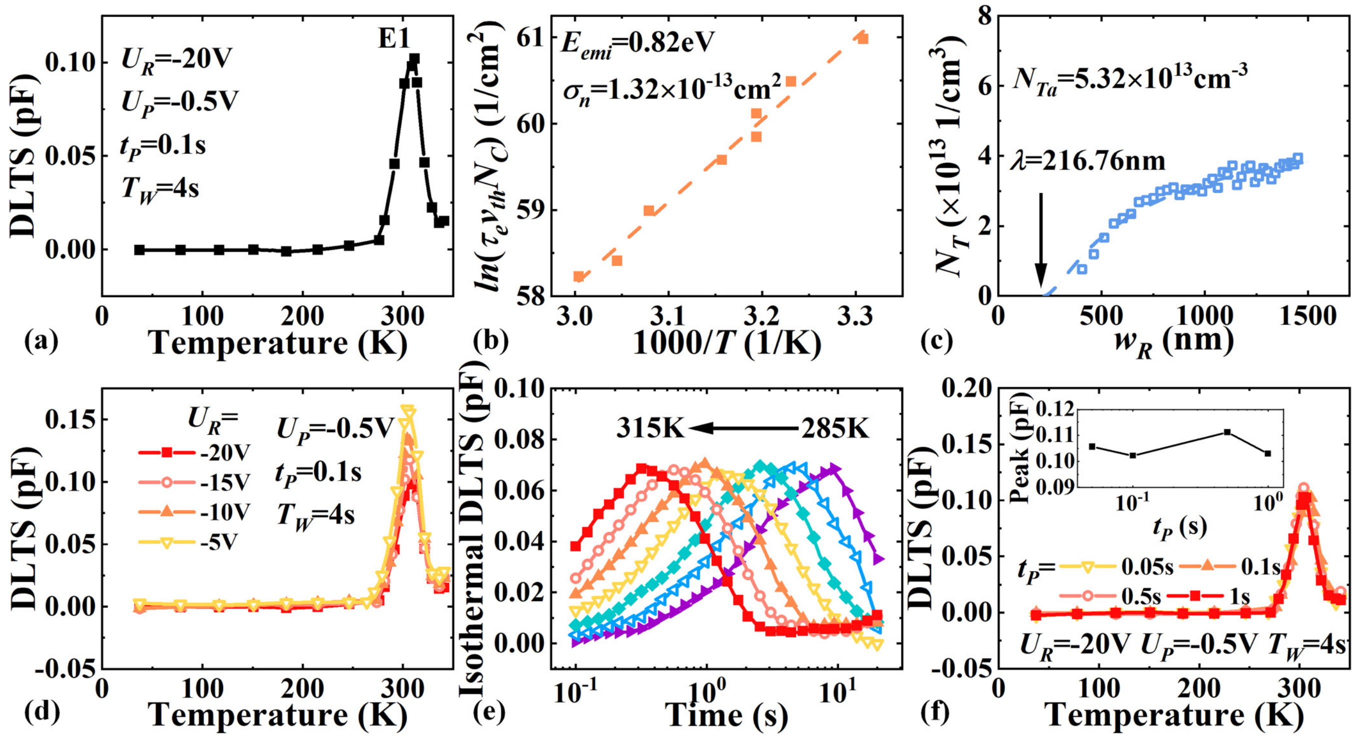


**FIG. 5.** (a) Temperature-scanning DLTS. (b) Arrhenius plot of E1. (c) Trap concentration ($N_T$) as a function of depletion region width with reverse bias ($w_R$). (d) With various $U_R$, temperature-scanning DLTS. (e) From 285 to 315 K, isothermal DLTS. (f) Temperature-scanning DLTS with various $t_P$. Inset: peak DLTS amplitude.



DLTS spectrum with a reverse bias $U_R = -20$ V, a filling pulse $U_P = -0.5$ V, a filling pulse width $t_P = 0.1$ s, and a measurement period $T_W = 4$ s. A majority carrier (electron) trap called E1 in this paper is revealed by a distinct peak around 305 K. Nevertheless, the DLTS signal reaches almost zero when the temperature is lower than 200 K, inferring that trap hardly affects the electrical performance of the $\beta$-$Ga_2O_3$ SBD at cryogenic temperature, matching well with the results in Figs. 3 and 4. It can be concluded that E1 is more likely to cause the dynamic performance and Lorentzian hump. As shown in Fig. 5(b), the activation energy for emission ($E_{emi}$) and capture cross section ($\sigma_n$) of E1 are extracted to be 0.82 eV and $1.32 \times 10^{-13}$ cm$^2$ by the Arrhenius plot. During the DLTS measurement, the depletion region width with a $U_R$ of $-20$ V is calculated to be 1.45 $\mu$m at 305 K, smaller than the thickness of the $\beta$-$Ga_2O_3$ homogeneous epilayer (7 $\mu$m). Therefore, the depletion region situates in the $\beta$-$Ga_2O_3$ epilayer, indicating that E1 is associated with a $\beta$-$Ga_2O_3$ homogeneous epilayer.

Figure 5(c) illustrates $N_T$ as a function of $w_R$. $N_T$ can be extracted from the capacitance transient amplitude ($\triangle C$) by the following equation:[29]

$$N_T = 2\frac{\Delta C}{C_R} N_S, \tag{6}$$

where $C_R$ denotes the capacitance with the bias of $U_R$ and $N_S$ donates the shallow donor concentration. The increase in $N_T$ with extending $w_R$ is attributed to the lambda effect, which claims that traps near the edge of the depletion region are unavailable to emit the electrons. Taking the lambda effect into account, the corrected trap concentration ($N_{Ta}$) can be derived by the following equation:[29]

$$N_T = N_{Ta}\left(1 - \frac{\lambda}{w_R}\right)^2, \tag{7}$$

where $\lambda$ represents the nonemission region width. From fitting, $N_{Ta}$ and $\lambda$ are calculated to be $5.32 \times 10^{13}$ cm$^{-3}$ and 216.76 nm, respectively.

E1 has been found in the $\beta$-$Ga_2O_3$ epilayer in our previous work, together with a similar $E_{emi}$ of 0.80 eV, a smaller $\sigma_n$ of $6.40 \times 10^{-15}$ cm$^2$, and a comparable $N_{Ta}$ of $4.95 \times 10^{13}$ cm$^{-3}$,[30] indicating that E1 has larger capture capability in this study. E1 is also widely found in other literature studies,[31–35] demonstrating the universality of E1 and the essentiality of characterization. According to the studies, E1 is found in samples before and after proton irradiation,[31,33] and E1 found in this work is considered to be compensating centers in $\beta$-$Ga_2O_3$ and is associated with complexes involving native defects.[31,33]

Figure 5(d) reports the temperature-scanning DLTS spectrum with different $U_R$. The positive peak corresponding to E1 stabilizes around 305 K, thereby supporting the conclusion that E1 is more likely to be a bulk trap rather than an interface trap.[36] Meanwhile, it can also be revealed that the emission process of E1 is independent of the electric field resulting from the fixed positive peak position.[36]

Figure 5(e) investigates the temperature-dependent emission process by isothermal DLTS from 285 to 315 K. The positive peak corresponding to the emission time constant ($\tau_e$) shifts toward a lower $T_W$ as the temperature increases. $\tau_e$ decreases from 8.98 s at 285 K to 0.35 s at 315 K, indicating a temperature-enhanced emission process.

Figure 5(f) displays the temperature-scanning DLTS spectrum with various $t_P$. It can be observed that the peak DLTS amplitude remains stable with increasing $t_P$, as shown in the inset in Fig. 5(f). The saturation of the peak DLTS amplitude demonstrates that traps are almost filled within a duration of 0.05 s.

## III. CONCLUSIONS

In summary, electrical properties of a relatively large-size ($2 \times 2$ mm$^2$) $\beta$-$Ga_2O_3$ SBD have been explicitly investigated for both room temperature and cryogenic temperature. Through *J*-*V* characteristics, *n* decreases from 1.34 at 50 K to 1.02 at 350 K, demonstrating the stable near-ideal Schottky characteristics. For leakage current characteristics, with a bias of −50 V, *J* at 100 K is one order of magnitude lower than that at 300 K, leading to outstanding blocking performance at low temperatures. From 50 to 350 K, $q\Phi_B$ extracted from *C*-*V* characteristics slightly declines from 0.70 to 0.65 eV. A variation in *J* can be readily observed during the stressing and recovery process at 300 K, while insignificant *J* fluctuation was recorded at 100 K. Meanwhile, a Lorentzian hump exists in low frequency noise spectra at 300 K but disappears at 100 K. The results of static characteristics, dynamic performance, and low frequency noise analysis point to high static performance and reliable switching properties of the $\beta$-$Ga_2O_3$ SBD at cryogenic temperature. The study establishes a solid foundation for the utilization of the large-size $\beta$-$Ga_2O_3$ SBDs as high power rectifiers for extreme low temperature environments.

## ACKNOWLEDGMENTS

This work was supported by ShanghaiTech University Startup Fund under Grant No. 2017F0203-000-14, the National Natural Science Foundation of China (Grant No. 52131303), the Natural Science Foundation of Shanghai (Grant No. 22ZR1442300), and, in part, by the CAS Strategic Science and Technology Program under Grant No. XDA18000000.

## AUTHOR DECLARATIONS

### Conflict of Interest

The authors have no conflicts to disclose.

### Author Contributions

Haolan Qu and Wei Huang contributed equally to this work.

**Haolan Qu:** Conceptualization (lead); Formal analysis (lead); Investigation (lead); Methodology (lead); Visualization (lead); Writing – original draft (lead); Writing – review & editing (equal). **Wei Huang:** Conceptualization (supporting); Methodology (supporting); Resources (equal); Writing – review & editing (supporting). **Yu Zhang:** Methodology (supporting); Writing – review & editing (equal). **Jin Sui:** Methodology (supporting); Writing – review & editing (supporting). **Jiaxiang Chen:** Writing – review & editing (supporting). **Baile Chen:** Methodology (supporting); Resources (supporting). **David Wei Zhang:** Methodology (supporting); Resources (supporting). **Yuangang Wang:** Methodology (supporting); Resources (supporting). **Yuanjie Lv:** Methodology (supporting); Resources (supporting). **Zhihong Feng:** Methodology (supporting); Resources (supporting). **Xinbo Zou:** Conceptualization (supporting); Funding acquisition (lead); Resources (equal); Supervision (lead); Writing – review & editing (equal).

## DATA AVAILABILITY

The data that support the findings of this study are available from the corresponding author upon reasonable request.

## REFERENCES


1. S. Pearton, F. Ren, M. Tadjer, and J. Kim, J. Appl. Phys. **124**, 220901 (2018).
2. K. D. Chabak *et al.*, Semicond. Sci. Technol. **35**, 013002 (2019).
3. H. Qu, J. Chen, Y. Zhang, J. Sui, R. Zhang, J. Zhou, X. Lu, and X. Zou, Semicond. Sci. Technol. **38**, 105010 (2023).
4. B. Wang, M. Xiao, J. Spencer, Y. Qin, K. Sasaki, M. J. Tadjer, and Y. Zhang, IEEE Electron Device Lett. **44**, 221 (2023).
5. Y. Zhang *et al.*, IEEE Trans. Electron Devices **67**, 3948 (2020).
6. H. Gong *et al.*, IEEE Trans. Power Electron. **36**, 12213 (2021).
7. Q. Yan *et al.*, Appl. Phys. Lett. **120**, 092106 (2022).
8. E. Farzana, A. Mauze, J. B. Varley, T. E. Blue, J. S. Speck, A. R. Arehart, and S. A. Ringel, APL Mater. **7**, 121102 (2019).
9. E. B. Yakimov *et al.*, APL Mater. **8**, 111105 (2020).
10. A. Y. Polyakov *et al.*, J. Phys. D: Appl. Phys. **53**, 274001 (2020).
11. M. E. Ingebrigtsen, A. Y. Kuznetsov, B. G. Svensson, G. Alfieri, A. Mihaila, U. Badstübner, A. Perron, L. Vines, and J. B. Varley, APL Mater. **7**, 022510 (2018).
12. J. Lee, E. Flitsiyan, L. Chernyak, J. Yang, F. Ren, S. J. Pearton, B. Meyler, and Y. J. Salzman, Appl. Phys. Lett. **112**, 082104 (2018).
13. F. Otsuka, H. Miyamoto, A. Takatsuka, S. Kunori, K. Sasaki, and A. Kuramata, Appl. Phys. Express **15**, 016501 (2022).
14. J. Kim, S. J. Pearton, C. Fares, J. Yang, F. Ren, S. Kim, and A. Y. Polyakov, J. Mater. Chem. C **7**, 10 (2019).
15. A. Jayawardena, A. C. Ahyi, and S. Dhar, Semicond. Sci. Technol. **31**, 115002 (2016).
16. J. Chen, H. Luo, H. Qu, M. Zhu, H. Guo, B. Chen, Y. Lv, X. Lu, and X. Zou, Semicond. Sci. Technol. **36**, 055015 (2021).
17. R. Sun, A. R. Balog, H. Yang, N. Alem, and M. A. Scarpulla, IEEE Electron Device Lett. **44**, 725 (2023).
18. C. De Santi, M. Fregolent, M. Buffolo, M. H. Wong, M. Higashiwaki, G. Meneghesso, E. Zanoni, and M. Meneghini, Appl. Phys. Lett. **117**, 262108 (2020).
19. P. K. Rao, B. Park, S.-T. Lee, Y.-K. Noh, M.-D. Kim, and J.-E. Oh, J. Appl. Phys. **110**, 013716 (2011).
20. K. R. Peta, B.-G. Park, S.-T. Lee, M.-D. Kim, J.-E. Oh, T.-G. Kim, and V. R. Reddy, Thin Solid Films **534**, 603 (2013).
21. K. Konishi, K. Goto, H. Murakami, Y. Kumagai, A. Kuramata, S. Yamakoshi, and M. Higashiwaki, Appl. Phys. Lett. **110**, 103506 (2017).
22. M. Higashiwaki *et al.*, Appl. Phys. Lett. **108**, 133503 (2016).
23. V. S. Nirwal and K. R. Peta, Mater. Res. Express **3**, 125901 (2016).
24. J. H. Werner and H. H. Güttler, J. Appl. Phys. **69**, 1522 (1991).
25. Z. Wang *et al.*, IEEE Trans. Electron Devices **69**, 981 (2022).
26. Y. Zhang, X. Zhang, M. Zhu, J. Chen, C. W. Tang, K. M. Lau, and X. Zou, IEEE Trans. Electron Devices **67**, 3992 (2020).

[27]M. Tang *et al.*, Appl. Phys. Lett. **123**, 013506 (2023).
[28]M. Zhu *et al.*, Microelectron. Reliab. **125**, 114345 (2021).
[29]K. Kanegae, M. Horita, T. Kimoto, and J. Suda, Appl. Phys. Express **11**, 071002 (2018).
[30]H. Qu *et al.*, Semicond. Sci. Technol. **38**, 015001 (2023).
[31]A. Y. Polyakov *et al.*, Appl. Phys. Lett. **112**, 032107 (2018).
[32]A. Y. Polyakov, I.-H. Lee, N. B. Smirnov, I. V. Shchemerov, A. A. Vasilev, A. V. Chernykh, and S. J. Pearton, J. Phys. D: Appl. Phys. **53**, 304001 (2020).
[33]A. Y. Polyakov, N. B. Smirnov, I. V. Shchemerov, D. Gogova, S. A. Tarelkin, and S. J. Pearton, J. Appl. Phys. **123**, 115702 (2018).
[34]Z. Zhang, E. Farzana, A. R. Arehart, and S. A. Ringel, Appl. Phys. Lett. **108**, 052105 (2016).
[35]M. E. Ingebrigtsen, J. B. Varley, A. Y. Kuznetsov, B. G. Svensson, G. Alfieri, A. Mihaila, U. Badstübner, and L. Vines, Appl. Phys. Lett. **112**, 042104 (2018).
[36]A. Coelho, M. Adam, and H. Boudinov, J. Phys. D: Appl. Phys. **44**, 305303 (2011).